Journal of Alloys and Compounds 829 (2020) 154553

Contents lists available at ScienceDirect

Journal of Alloys and Compounds

journal homepage: http://www.elsevier.com/locate/jalcom

Correlation between partial inhibition of hydrogen evolution using thiourea and catalytic activity of AB5-type hydrogen storage alloy towards borohydride electrooxidation

Małgorzata Graś [a], Jarosław Wojciechowski [a], Katarzyna Lota [b], Tomasz Buchwald [c], Jacek Ryl [d], Grzegorz Lota [a, b, *, 1]

[a] Institute of Chemistry and Technical Electrochemistry, Poznan University of Technology, Berdychowo 4, 60-965, Poznan, Poland
[b] Łukasiewicz Research Network - Institute of Non-ferrous Metals Division in Poznan Central Laboratory of Batteries and Cells, Forteczna 12, 61-362, Poznan, Poland
[c] Institute of Material Research and Quantum Engineering, Poznan University of Technology, Piotrowo 3, 60-965, Poznan, Poland
[d] Department of Electrochemistry, Corrosion and Materials Engineering, Faculty of Chemistry, Gdansk University of Technology, Narutowicza 11/12, 80-233, Gdansk, Poland

ARTICLE INFO

Article history:
Received 7 January 2020
Received in revised form
19 February 2020
Accepted 26 February 2020
Available online 29 February 2020

Keywords:
Hydrogen absorbing materials
Metals and alloys
Surfaces and interfaces
Corrosion
Electrochemical reactions
Fuel cells

ABSTRACT

Direct borohydride fuel cells (DBFCs) are devices which directly convert the chemical energy stored in the borohydride ion and oxidant into electrical energy as a result of redox reactions. Unfortunately, a significant amount of fuel is lost as a result of the undesirable hydrolysis reaction. The selection of an efficient borohydride hydrolysis inhibitor requires detailed knowledge regarding the interaction mechanism between the inhibitor molecule and electrode surface. In this study, various amounts of thiourea additives (0.011−1.600 mM) were tested to select the best fuel composition for DBFC application. When AB_5-type anode was used, only partial inhibition of sodium borohydride hydrolysis was a desirable phenomenon. Partially released hydrogen results in the improvement of catalytic properties of the alloy. The addition of 0.016 mM thiourea does not inhibit the oxidation of borohydride, on the contrary, it increases the practical capacity from 27% to 41% of the theoretical value. Moreover, we indicate that the addition of thiourea prevents corrosion as well as degradation of the electrode surface. Pressure measurements confirmed the effectiveness of thiourea in relation to hydrogen evolution, while X-ray photoelectron spectroscopy and Raman spectroscopy revealed that the electrode surface was not poisoned.

1. Introduction

The growing human population consumes more energy than ever before in history. It is predicted that in 2035 the demand for electricity will increase almost twice compared to 2008 [1]. According to the International Partnership for Hydrogen and Fuel Cells in the Economy (IPHE), fuel cells are important solutions for large-scale and long-term storage. These devices can help in effective decarbonization of our energy systems [2].

Currently, the Proton Exchange Membrane Fuel Cell (PEMFC) is the most technologically advanced fuel cell system. However, this type of fuel cell is also characterized by some drawbacks: (i) very acidic perfluorosulfonic proton exchange membrane renders it necessary to use non-corrodible materials, which are inherently costly; (ii) PEMFC must be fed with ultra-pure hydrogen (for example, obtained by electrolysis of water) or steam reforming of natural gas [3,4]. Bipolar plates are crucial components of PEMFC power stack. D. Kong et al. have noticed that after heat treatment, the proportion of oxides in passive layer formed on SLM 316L increases, which leads to better anti-corrosion properties [5]. The authors also studied the effect of hydrogen charging on the microstructure and durability of traditional wrought and selective laser melted 316L stainless steels. Researchers used thiourea to prevent the formation of a hydrogen molecule during hydrogen charging [6].

* Corresponding author. Institute of Chemistry and Technical Electrochemistry, Poznan University of Technology, Berdychowo 4, 60-965, Poznan, Poland.
E-mail address: grzegorz.lota@put.poznan.pl (G. Lota).
[1] ISE member.

https://doi.org/10.1016/j.jallcom.2020.154553

Direct borohydride fuel cell (DBFC) is fed with an aqueous alkaline solution of borohydride. Borohydrides (MBH_4, M = Na, K, Li) are attractive chemical compounds because they are chemically stable and not flammable [7]. Metal hydride compressors allow to replace the liquid or compressed hydrogen fuel tanks by a solid fuel tank [8]. DBFC generally uses sodium borohydride as a fuel, because $NaBH_4$ offers a high specific energy density (9.3 Wh g^{-1}) owing to its high hydrogen content (10.8 wt%) [9]. Direct borohydride fuel cell converts the chemical energy stored in the borohydride ion (Eq. (1)) [10]:

$$BH_4^- + 8\ OH^- \rightarrow BO_2^- + 6\ H_2O + 8\ e^- \cdot E^0 = -1.24\ \text{V vs.NHE} \quad (1)$$

The standard potential of reaction (1) is equal to −1.24 V vs. NHE, which means that it is possible to achieve a value more negative by approx. 0.41 V than in the case of hydrogen electrode in an alkaline medium [11]:

$$H_2 + 2\ OH^- \rightarrow 2\ H_2O + 2\ e^- \cdot E^0 = -0.83\ \text{V vs.NHE} \quad (2)$$

Unfortunately, a significant amount of fuel is lost as a result of the hydrolysis reaction, which leads to the formation of hydrogen (Eq. (5)) and, consequently, to the reduced utilization of borohydride.

$$BH_4^- + H_2O \rightarrow BH_3(OH)^- + H_2 \cdot \quad (3)$$

$$BH_3(OH)^- + H_2O \rightarrow BO_2^- + 3\ H_2 \cdot \quad (4)$$

$$BH_4^- + 2\ H_2O \rightarrow BO_2^- + 4\ H_2 \cdot \quad (5)$$

Most studies are focused on finding appropriate anode catalysts (CoO, Pd-Cu, Pt/Ti_2O, Pd/C) to achieve maximum electron transfer (i.e. $8e^-$) [12–14]. Unfortunately, highly active borohydride oxidation catalysts are also highly active toward the borohydride hydrolysis. The rare-earth-based, AB_5-type hydrogen storage alloys possess the ability to absorb hydrogen at room temperature, therefore they are a very interesting group of anode materials for DBFC [15–18]. For fuel cell application, the formation of the hydride phase may affect both the catalytic activity and the structural stability of the electrode. The processes of alloy hydriding, either chemically or electrochemically, can be attributed to the electrooxidation of the hydride introduced into the alloy during activation [19].

Another method to limit the rate of hydrogen evolution is to add thiourea to the fuel solution, as proposed by Gyenge [20]. The interaction of thiourea on platinum electrode was questioned by Demirci. The author suggested, that sulfur species can cause deactivation of metallic surface by creating strong metal-sulfur bonds [21]. The interaction of thiourea on gold [22,23], platinum [24–26], copper [27,28] and silver [28–30] electrodes in different solutions was the topic of number of electrochemical and spectroscopic studies. For instance, R. Jamard et al. have reported that the addition of 10^{-4} M thiourea into 2 M $NaBH_4$ and 1 M NaOH enhanced the coulombic efficiency of DBFC from 18% to 64% using

Table 1
Nomenclature of analyzed systems with thiourea content.

Abbreviation of fuel solution	Dilution	Final concentration (mM)
T1	–	1.600
T50	T1/50	0.032
T100	T1/100	0.016
T150	T1/150	0.011
T0 (thiourea zero)	–	–

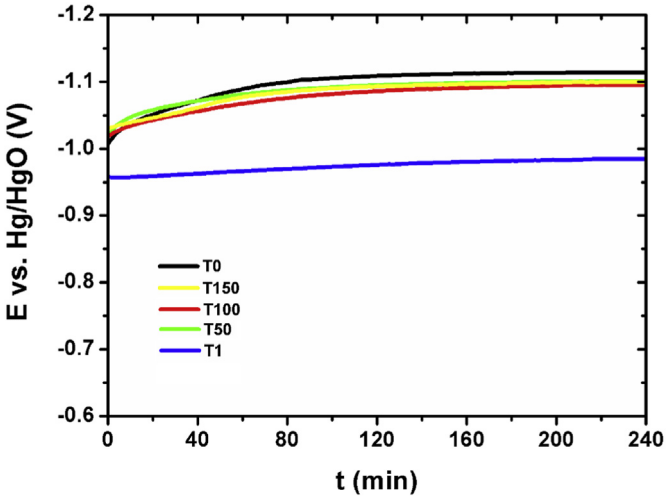

Fig. 1. Open circuit potential versus time of AB_5-type anodes supplied with different concentrations of thiourea in 0.5 M $NaBH_4$ + 6 M KOH.

Pt anode However, after thiourea addition, OCV was lower, which led to decrease in DBFC power [10]. C C. Celik et al. have studied the addition of thiourea in steady state/steady-flow and uniform state/uniform-flow systems to minimize the anodic hydrogen evolution on Pd/C electrode. The power density increased from 14.4 to 15.1 mW cm^{-2} [31]. V.W.S. Lam et al. have experimentally confirmed, using the electrochemical quartz crystal microbalance technique, that at thiourea concentrations higher than 0.045 mM (with reference to 30 mM BH_4^-) increases the overpotential of borohydride electrooxidation on Pt, inhibiting the hydrolysis reaction [32]. Atwan et al. have studied the oxidation of sodium borohydride in the presence of thiourea on Os nanoparticles. Based on half-cell tests, it was found that thiourea is oxidized at a potential of about 0 V vs. Ag/AgCl, KCl_{std}. However, it is uncertain, whether the accumulation of thiourea oxidation products would poison the Os catalyst in DBFC [33,34]. Therefore, further research is still required in both, surface techniques and fuel cell experiments to clarify the inhibition mechanism of hydrolysis and possible long-term poisoning of the catalyst by thiourea. This paper discusses the correlation between partial inhibition of hydrogen evolution and catalytic activity of AB_5-type hydrogen storage alloy towards

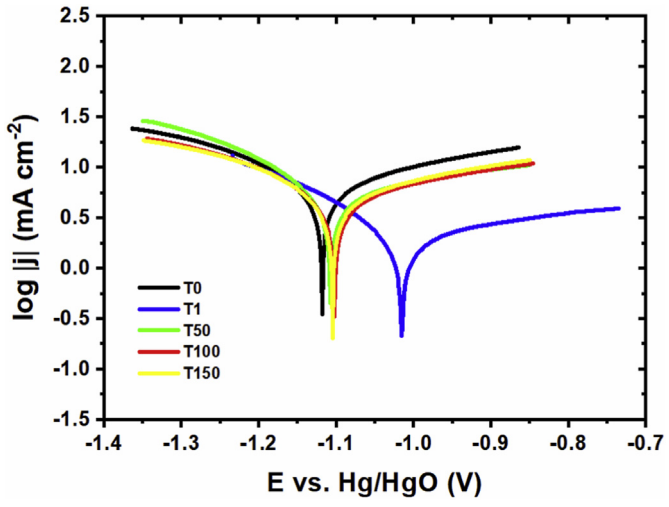

Fig. 2. Potentiodynamic polarization curves of all tested electrolytes.

borohydride electrooxidation, which is essential to improve the catalytic fuel processing. To the best of our knowledge such studies have not be performed before. The effective use of AB_5-alloy-based electrode for DBFC application in the presence of thiourea remains without a clear response. The innovative research presented in the framework of this study concerns the impact of inhibition of hydrogen evolution by thiourea on the effectiveness of borohydride oxidation reaction and, at the same time, on the formation of the hydride phase. Additionally, we have also reported changes in the internal pressure profiles in the half-cell for the first time, which depend on the amount of thiourea added.

2. Experimental

2.1. Electrode materials and chemicals

The materials and chemicals used during the tests are listed as follows: $NaBH_4$ (99%, Acros Organics), KOH (85%, POCH), $(NH_2)CS$ (≥99%, Sigma-Aldrich), Ni foam (Changsha LYRUN New Material Co.,Ltd), $LaMmNi_{3.55}Al_{0.30}Mn_{0.40}Co_{0.75}$ (≥99.5% Stanchem, Treibacher, Aldrich), 255-type carbonyl nickel powder (Inco, 99.9%), graphite powder (Lonza), PVA (M.W. 115,000 ≥ 88%,VWR).

2.2. Materials preparation

The details regarding the preparation of anodes have been described in our previous publication [35]. AB_5-type hydrogen storage alloy with addition of nickel carbonyl and graphite was distinguished by the best catalyst activity regarding sodium borohydride oxidation, therefore we selected it for further experiments.

2.3. Electrochemical measurements

Electrochemical measurements were performed in a three-electrode configuration. The AB_5-type anode was used as the working electrode, while nickel foam and Hg/HgO were used as the counter and reference electrodes, respectively. All the electrochemical tests were carried out in a 6 M KOH solution containing 0.5 M of $NaBH_4$ with different amounts of thiourea. The electrodes have been immersed into a 60 mL of fuel solution. At first, the influence of thiourea (TU) on the anti-corrosive properties of DBFC anode was estimated. Therefore, potential at open circuit conditions (OCP) was measured (4 h), followed by potentiodynamic polarization (PP) test. PP study was performed to determine the corrosion potential (E_{corr}) and corrosion current density (j_{corr}). The working electrode was first polarized cathodically to −250 mV and then anodically to 250 mV, twice vs. OCP. The anodic scan rate was equal to 0.2 mV s^{-1}. The impact of inhibition of hydrogen evolution by thiourea on the effectiveness of borohydride oxidation reaction was investigated using chronopotentiometric measurements with the constant current density of 1 mA g^{-1} and 100 mA g^{-1} (calculated based on the active mass of electrode), cyclic voltammetry (CV) and electrochemical impedance spectroscopy (EIS) (6.3 mHz - 100 kHz). All electrochemical tests were carried out at ambient temperature using potentiostat/galvanostat VMP3 (BioLogic, France), equipped with the impedance module. The gas evolution was detected with a digital pressure sensor KELLER 33X (pressure range 0–3 bars with total error band of 0.05%).

To obtain a full insight into the electrode behavior in the presence of thiourea (TU), four different concentrations were tested. Table 1 presents the content of thiourea in a 0.5 M $NaBH_4$ + 6 M KOH solution.

Table 2
Corrosion potential (E_{corr}), corrosion current density (j_{corr}) and slopes of anodic (β_a) and cathodic (β_c) polarization curves values estimated from potentiodynamic polarization measurements. All the values were estimated using EC-Lab® Software.

Fuel solution	E_{corr} (mV vs Hg/HgO)	j_{corr} (mA cm^{-2})	β_a (mV)	$-\beta_c$ (mV)
T0	−1119	39.0	534	241
T1	−1015	3.56	1044	159
T50	−1107	26.5	1005	177
T100	−1102	26.5	826	251
T150	−1105	31.2	837	279

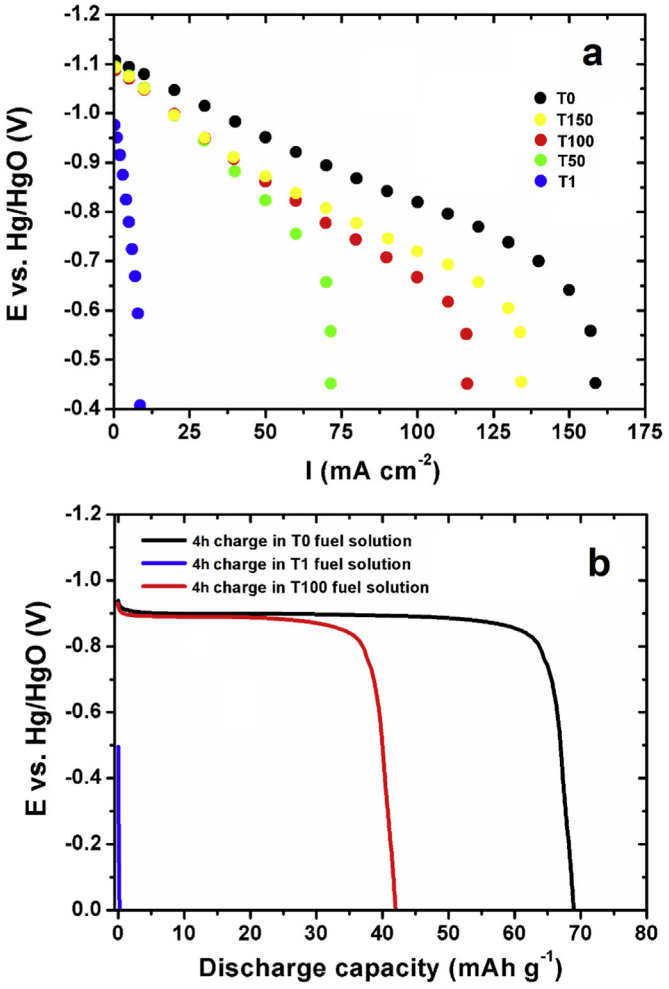

Fig. 3. (a) Potential-current curves for different concentrations of thiourea in 0.5 M $NaBH_4$ + 6 M KOH (b) Chronopotentiometry curves in 6 M KOH (I = 1 mA g^{-1}) of AB_5-type anodes previously exposed for 4 h to T0, T1 and T100 fuel solution.

2.4. Materials characterization

Surface morphology and physicochemical analyses of working electrodes were carried out using a Scanning Electron Microscope (Quanta 250 FEG, FEI) equipped with Energy Dispersive X-ray spectrometer (EDX). 3D surface measurements were analyzed using the VHX-7000 series (Keyence) digital microscope. The X-ray diffraction method (XRD) with CuKα radiation wavelength of 1.5418 Å (Philips, PW 1050) was used to examine the structure of alloys. All measurements were recorded at an angle (2θ) range of 20–80°. AB_5-type anodes were also analyzed by Raman spectroscopy, which were carried out using an inVia Renishaw micro-

Raman system with a diode-pumped laser that emits a 785 nm wavelength. After electrochemical measurements, the electrodes were also subjected to XPS analysis (Escalab 250Xi, ThermoFisher Scientific) which was performed with Al Kα radiation (1486.7 eV). The pass energy was equal to 20 eV and spot size was at 650 μm. The spectra were deconvoluted by applying GaussianLorentzian line-shapes with Smart® background, the feature implemented in Avantage software (ThermoFisher Scientific).

3. Results and discussion

3.1. Electrochemical measurements

In the first step, measurements were carried out in a borohydride alkaline solution (0.5 M $NaBH_4$ + 6 M KOH), which was selected as the reference system (T0) in order to estimate the influence of different amounts of thiourea on the electrochemical performance.

Fig. 1 shows the OCP vs. time of anode materials for different types of fuel solutions. The OCP values were equal to −1.10 V (T0), −0.96 V (T1) and c.a. −1.08 V vs. Hg/HgO for subsequent dilutions of the T1 system, i.e. T50, T100 and T150. Although the OCP of all types of fuel solutions were less negative than the theoretical BH_4^-/BO_2^- equilibrium potential (−1.34 V vs. Hg/HgO), they were significantly lower than the potential of hydrogen electrode in the alkaline medium, which confirms the activity of AB_5-alloy-based electrode for the borohydride oxidation reaction. Moreover, as can be observed after analysis of the curve, the OCP for T1 system is equal to approx. −0.96 V when the electrode is immersed in the solution and this value does not decrease within 2 h. This indicates that the surface state does not change dramatically, which could happen if thiourea was decomposed to sulphide.

The results of PP tests were presented in Fig. 2, while the analysis data in Table 2. Corrosion potential (E_{corr}), corrosion current density (j_{corr}) and slopes of anodic (β_a) and cathodic (β_c) polarization curves values were estimated using EC-Lab® Software. The T1 system was characterized by the highest and lowest corrosion potential and corrosion current density values, respectively. The other types of electrolytes demonstrated slightly lower corrosion potentials and higher corrosion current densities. It is well known, that the corrosion process of an alloy depends on the chemical composition of the material, its microstructure, the nature of electrolyte and cycling conditions [36–40]. The presence of a lone pair of electrons in the inhibitor molecule (TU) allows for electron transfer from an inhibitor to the metal, leading to the formation of a coordinate covalent bond [41]. This was most likely caused by the formation of a protective film on the anode surface through thiourea adsorption. The shift of OCP and E_{corr} values towards more positive values may suggest that the thiourea additive acts as an anodic corrosion inhibitor.

The potential-current characteristics of the anode system were presented in Fig. 3a. It can be observed, that the polarization performance strongly depended on the thiourea concentration in 0.5 M $NaBH_4$ + 6 M KOH. In case of T1 fuel solution, the reduced surface activity of the electrode is evident. It should be noted that AB_5-alloy based electrode immersed in the borohydride solution without the addition of thiourea exhibited the highest oxidation currents. This is most likely due to the continuous hydrolysis of borohydride, which results in the production of large amounts of hydrogen and allows for greater insertion of hydride into the alloy.

The experiment in which the electrodes were charged by immersion in borohydride solution for 4 h with different concentrations of thiourea confirmed the above-mentioned information (Fig. 3b). When the AB_5-alloy-based electrode was used as the anode catalyst for borohydride oxidation, our results confirmed that the hydrogen storage alloy is able to absorb hydrogen during immersion in T0 and T100 electrolytes. The hydrogen produced may be stored in the form of metal hydride or released in the form of gas bubbles, when the rate of hydrolysis reaction is higher than the rate of hydride absorption [42]:

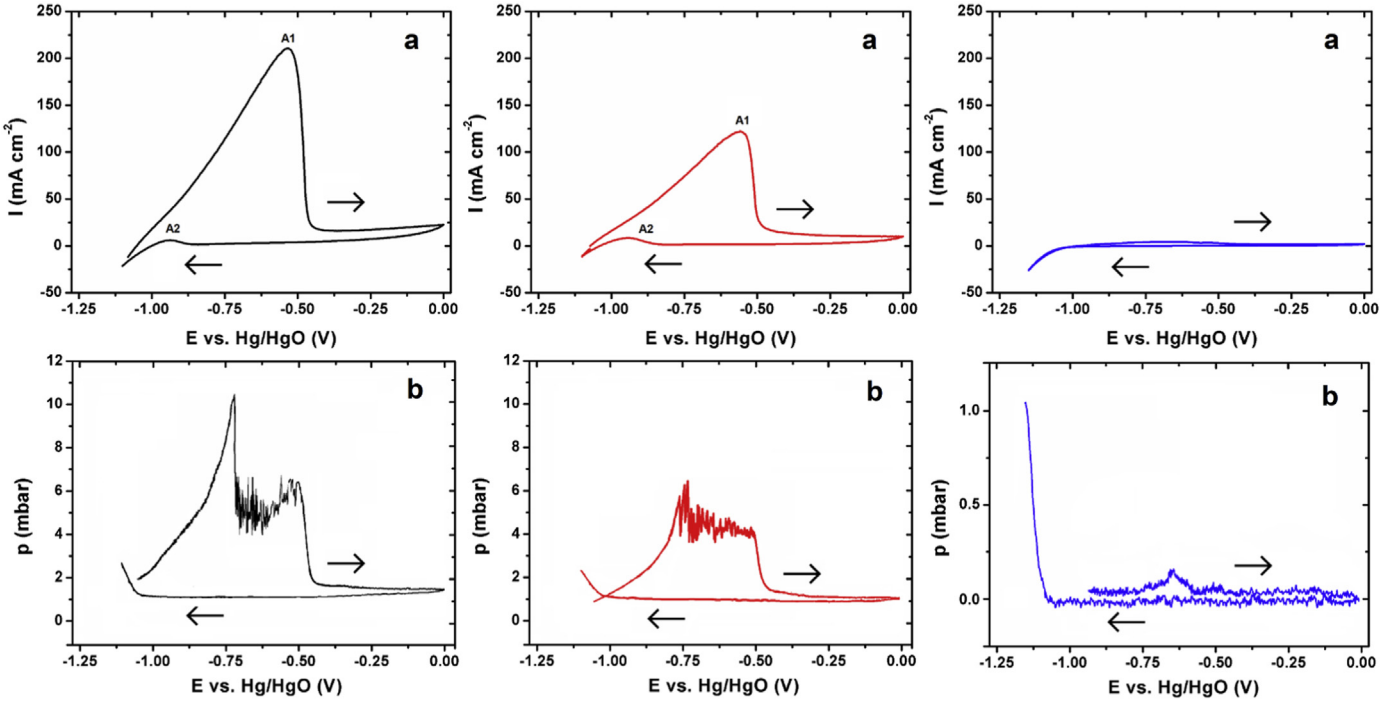

Fig. 4. (a) Voltammetric responses with a scan rate of 5 mV s^{-1} (b) Pressure profiles for AB_5-type anodes supplied with T0, T100 and T1 fuel solutions.

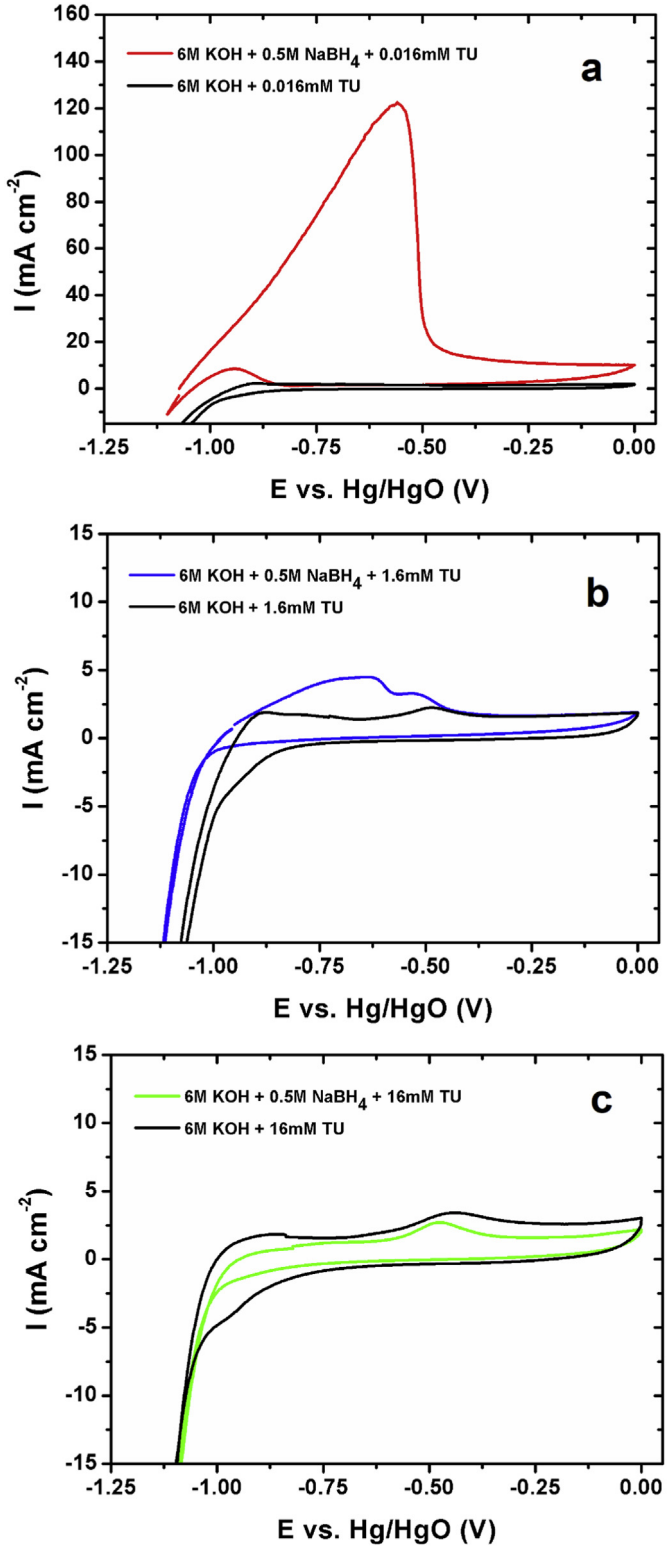

Fig. 5. Effect of thiourea (TU) concentration on the voltammetric responses of AB_5-type anodes (a) 0.016 mM TU (b) 1.6 mM TU (c) 16 mM TU.

$$BH_4^- + 2\,H_2O + 8\,M \leftrightarrow BO_2^- + 8\,MH_{ads} \quad (6)$$

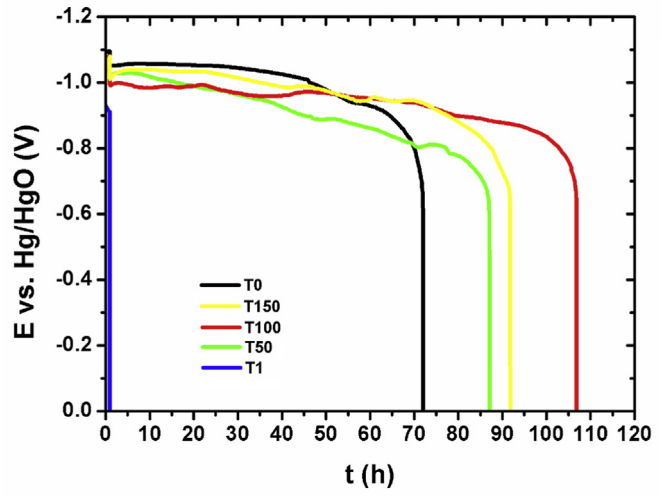

Fig. 6. Chronopotentiometry curves (I = 100 mA g^{-1}) of AB_5-type anodes supplied with different concentrations of thiourea in 0.5 M $NaBH_4$ + 6 M KOH.

$$MH_{ads} \leftrightarrow MH_{abs} \quad (7)$$

$$MH_{ads} \leftrightarrow 1/2\,H_2 + M \quad (8)$$

These investigations indicate that there is a very good prospect for the application of these materials as anodes for DBFC. In case of T100 fuel solution, the AB_5-alloy-based anode appeared to be less active towards the hydrolysis reaction (compared to T0 fuel solution), therefore, as expected, less gas was released from the electrode resulting in a lower hydride charge.

The internal pressure of anode systems supplied with 60 mL of T1, T100 and T0 fuel solution was determined using a pressure sensor to follow hydrogen evolution during the oxidation of sodium borohydride. The results were presented in Fig. 4. The top pictures

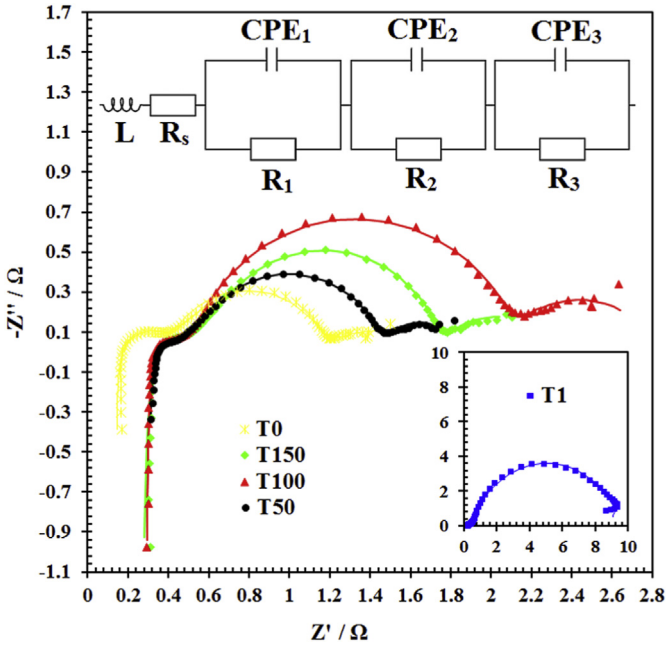

Fig. 7. Nyquist plots of all tested systems and electrical equivalent circuit used for fitting the EIS data. Raw data (symbols) and fitted data (solid lines).

Table 3
Inductance (L), resistance (R) and constant phase element (CPE) values of electrical equivalent circuit components, matched to Nyquist plots. All the values were estimated using EC-Lab® Software.

Fuel solution	$L \cdot 10^{-6}$ (H)	R_s (Ω)	CPE_1 (F $s^{(\alpha-1)}$)	R_1 (Ω)	CPE_2 (F $s^{(\alpha-1)}$)	R_2 (Ω)	CPE_3 (F $s^{(\alpha-1)}$)	R_3 (Ω)
T0	0.64	0.14	0.001	0.27	0.018	0.75	6.99	0.55
T1	0.02	0.28	0.018	0.25	0.046	8.74	16.29	0.09
T50	0.55	0.28	0.171	0.36	0.051	0.86	19.46	0.34
T100	1.51	0.29	0.013	0.25	0.036	1.58	8.37	0.70
T150	1.53	0.23	0.098	0.50	0.037	1.04	17.55	0.53

(Fig. 4a) demonstrate the borohydride oxidation current densities (CV curves). Potential scanning was performed from open-circuit potential to 0.00 V in the anodic region and then the scan was reversed in the cathodic direction to −1.15 V. The bottom pictures (Fig. 4b) represent the pressure profiles, which are proportional to the rate of H_2 formation. During the scanning process to more positive potentials, the generation of hydrogen occurred as a result of borohydride hydrolysis, therefore a continuous pressure increase in T0 (black line) and T100 (red line) systems was observed. Two oxidation peaks were observed for these types of fuels. The broad peak A1 visible at the potential value of c.a. −0.6 V vs. Hg/HgO could be attributed to desorption of hydrogen atoms from the electrode surface and due to the direct oxidation of borohydride [43]. In the absence of thiourea, the profile of pressure formation during borohydride oxidation suggests that hydrogen may also be formed as a by-product of this reaction (reactions (3) and (4)). The second anodic peak (A2), which appears at c.a. −1.0 V in the reverse cycle, could be mainly assigned to BH_3OH^- oxidation [44]. There is also a quantitative difference in gassing when the T100 fuel solution was used, which confirms that this amount of thiourea has a beneficial effect on the inhibition of borohydride hydrolysis, because it does not interfere with borohydride oxidation. In case of T1 fuel solution (blue curve), it was observed that peaks A1 and A2 disappear. The pressure profile stabilizes with the change of the electrode potential, which indicates complete inhibition of borohydride oxidation and hydrolysis processes. This means that such a high concentration of thiourea has a negative impact on the performance of this system by decreasing the current density associated with borohydride oxidation. Thiourea strongly adsorbs on the anode surface, therefore some AB_5-type hydrogen storage alloy sites are not accessible for oxidation, which is in good agreement with our previous results. A significant change in the pressure profile was only observed due to the cathodic discharge of water.

In order to determine the effects of thiourea concentration on the borohydride oxidation, additional cyclic voltammetry tests were carried out (Fig. 5a–c). The voltammogram obtained for T100 system (0.016 mM TU) confirms that this amount of TU does not restrict the borohydride electrooxidation. However, we decided to significantly increase the concentration of thiourea (up to 16 mM) just to understand the mechanism of the oxidation reaction. After increasing the thiourea concentration, it can be observed that current density associated with the peak at c.a. −0.5 V vs. Hg/HgO is lower than that observed only with thiourea in 6 M KOH. With such a high concentration of thiourea, there is a competition between

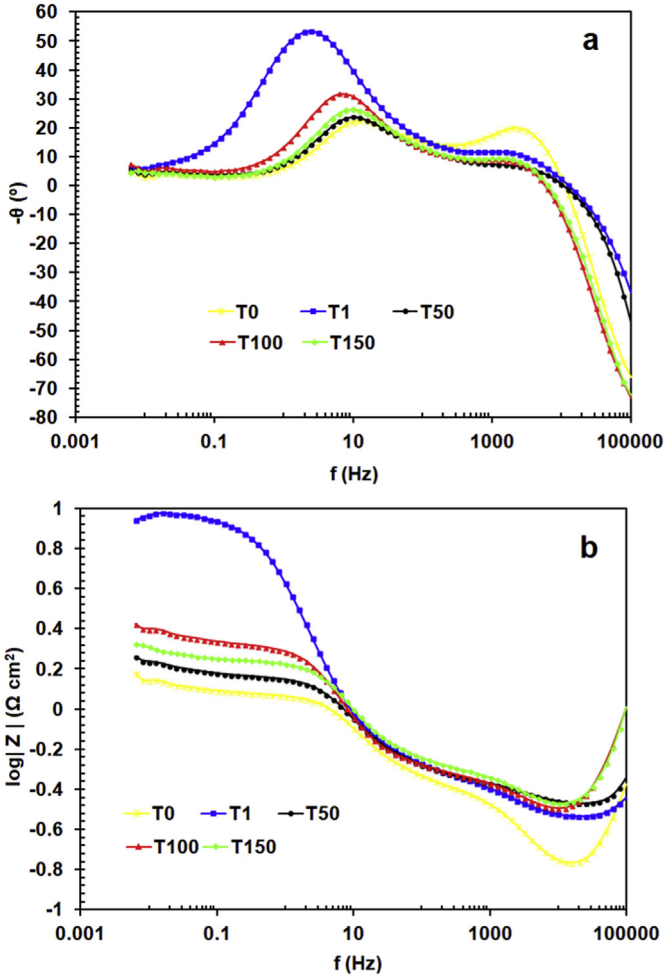

Fig. 8. Bode plots of all tested systems. Raw data (symbols) and fitted data (solid lines). (a) Phase angle (b) Impedance modulus.

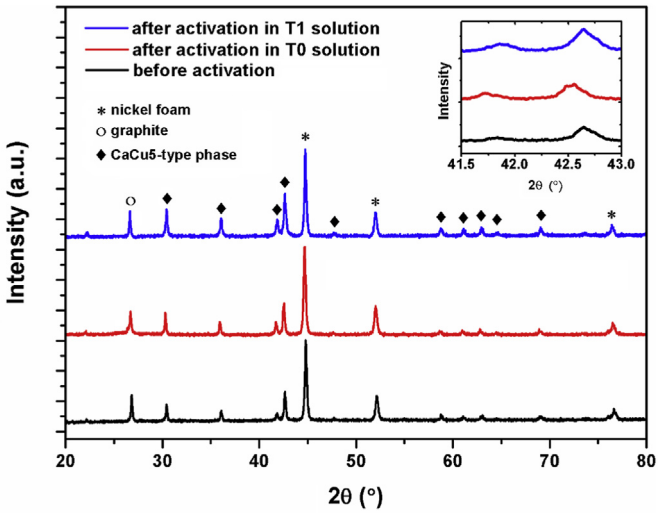

Fig. 9. XRD patterns of AB_5-type anodes before (black line) and after activation in T1 fuel solution (blue line) and T0 fuel solution (red line). (For interpretation of the references to colour in this figure legend, the reader is referred to the Web version of this article.)

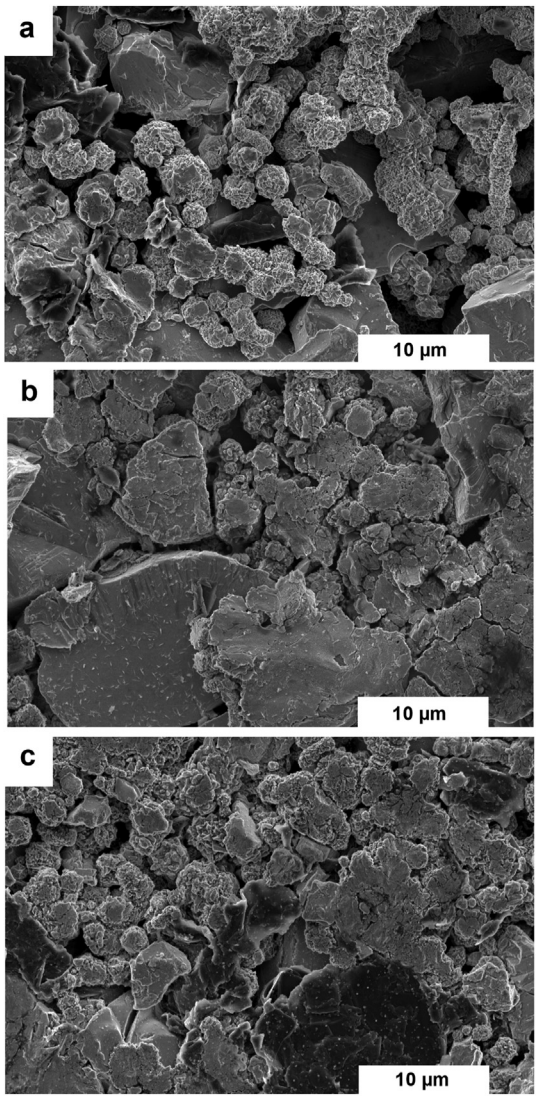

Fig. 10. SEM images of AB_5-type anodes before (a) and after 4 h activation in T0 (b) and T1 (c) electrolytes.

the oxidation of TU and BH_4^-, which is in good agreement with results of Martins et al. [45]. It is well known that in acidic and neutral media thiourea is oxidized to formamidine disulphide according to the following reaction [46]:

$$2\,H_2NC(S)NH_2 \leftrightarrow HN=C(NH_2)S-SC=NH(NH_2)+2e^- + 2H^+ \quad (9)$$

Considering the data reported by Vandeberg et al. [47], it can be assumed that the anodic peak at c.a. −0.5 V vs. Hg/HgO can also correspond to the one-electron oxidation of thiourea. Unfortunately, in an alkaline medium this disulfide is unstable which can result in the formation of atomic sulfur [48].

The chronopotentiometric curves of the anode systems supplied with 60 mL of fuel solution with different concentrations of thiourea were presented in Fig. 6. In this case, it is theoretically possible to store a 6.3 Ah charge, assuming a maximum electron transfer. In the absence of thiourea (T0) the anode potential is stabilized at c.a. −1.05 V vs. Hg/HgO in the first 50 h, and then a sharp decrease is observed. Fuel solution without thiourea was characterized by very low coulombic efficiency because of the parallel hydrolysis reaction. The measured capacity was equal to 1.7 Ah, which is approximately equal to 27% of the theoretical value. In case of T100 fuel solution, the anode potential is maintained at approx. −0.95 V vs. Hg/HgO for about 100 h. The measured capacity was equal to 2.5 Ah, which is approximately equal to 41% of the theoretical value. This may suggest that hydrogen molecules produced as a result of the minimized, but still partly present borohydride hydrolysis contribute to the improvement of AB_5-alloy-based anode activation properties.

During the *ex situ* measurements, electrochemical impedance spectroscopy served to characterise the materials used in DBFC. The electrochemical impedance spectroscopy results (Nyquist plots) of all tested systems were presented in Fig. 7. Electrical equivalent circuits (EEC) were matched using EC-Lab® Software. Symbols and solid lines represent raw and fitted data, respectively. The EEC is composed of an inductive element (L), an equivalent series resistance (R_s), and three CPE/R time constants. The first of these elements (L) describes the magnetic phenomena (negative values of −Z''), the second (R_s) expresses the resistance of the electrolyte solution in which all the electrochemical tests were performed. The remaining three time constants represent two elements connected in parallel, i.e. CPE (constant phase element) and R (resistor). The first one expresses the capacitance of a non-ideal capacitor. The

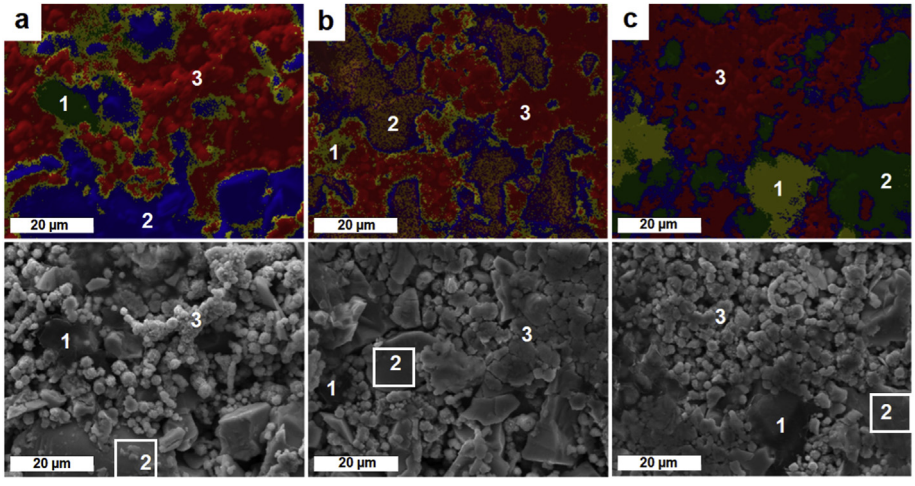

Fig. 11. EDS analysis of AB_5-type anodes before (a) and after 4 h activation in T0 (b) and T1 (c) electrolytes.

Table 4
Chemical composition of marked areas in Fig. 11 in wt. %.

Area	Ni	Co	Mn	Nd	Pr	Ce	La	Al	O
2a	43.3 ± 0.6	3.3 ± 0.1	1.4 ± 0.1	1.1 ± 0.1	0.6 ± 0.1	2.5 ± 0.1	3.3 ± 0.1	0.2 ± 0.03	10.5 ± 1.7
2b	32.6 ± 0.4	1.8 ± 0.1	0.8 ± 0.1	0.8 ± 0.1	0.6 ± 0.1	1.5 ± 0.1	2.0 ± 0.1	1.5 ± 0.1	30.0 ± 4.7
2c	34.7 ± 0.5	2.0 ± 0.1	0.9 ± 0.1	0.5 ± 0.1	0.2 ± 0.04	1.7 ± 0.1	2.5 ± 0.1	0.1 ± 0.02	26.4 ± 4.1

second describes the resistance. CPE presence (instead of a capacitor) is associated with capacitive dispersion at the electrode/electrolyte interface. This is caused by slow ion adsorption and surface chemical heterogeneity [49]. Table 3 contains all EEC components values, which were determined using EC-Lab® Software. The obtained EIS results confirmed the previous assumptions. The Nyquist plots showed three loops (or semicircles). The first time constant (high-frequency time constant) corresponds to the first loop and presents the resistive and capacitive phenomena of various types of electrical connections, including the connection between the working and reference electrodes [50]. Values of the resistance elements constituting the first time constant were similar for all the presented systems, which confirms that it is not a reflection of the occurrence of electrochemical phenomena. In addition, all systems containing thiourea were characterised by an identical value of the equivalent series resistance (R_s). The electrolyte solution without the addition of thiourea (T0) exhibited the highest conductivity (lowest R_s). The second time constant (CPE_2/R_2) refers to the adsorption processes of hydrogen atoms on the electrode surface as well as to the electrochemical reactions [50]. In this case, there were remarkable differences between all tested samples. The highest value of resistance R_2 was exhibited by the T1 system with the greatest amount of added thiourea. As mentioned previously, the presence of 1.6 mM TU caused an almost complete blockage of the free sites on the electrode surface for electrochemical reactions involving hydrogen. In case of the remaining systems, the highest value of the charge transfer resistance, included in R_2, was exhibited by the sample T100 (0.016 mM TU). Based on the results of direct current methods, such an amount of TU has been considered as optimal, i.e. such an amount of TU results in effective blocking of available sites for borohydride hydrolysis, making the direct oxidation of borohydride more favourable. Therefore the value of R_2 increases, while CPE_2 decreases. In the system without thiourea, all the processes discussed above were most rapid. The third time constant (CPE_3/R_3) refers to the diffusion of hydrogen atoms in the AB_5-alloy-based anode [50]. The R_3 and CPE_3 values was highest and lowest for T100, respectively. As mentioned above, the addition of 1.6 mM of thiourea resulted in an almost complete inhibition of the electrode/electrolyte interface reactions. This could be caused by the formation of intermediate, thermodynamically unstable products, which is indicated by the negative capacitive loop in the low frequency range.

The Bode plots of all tested samples were presented in Fig. 8a and b. In the high frequency range, values of the phase angle and the impedance modulus were positive and negative, respectively. This is a reflection of the occurrence of magnetic phenomena in the

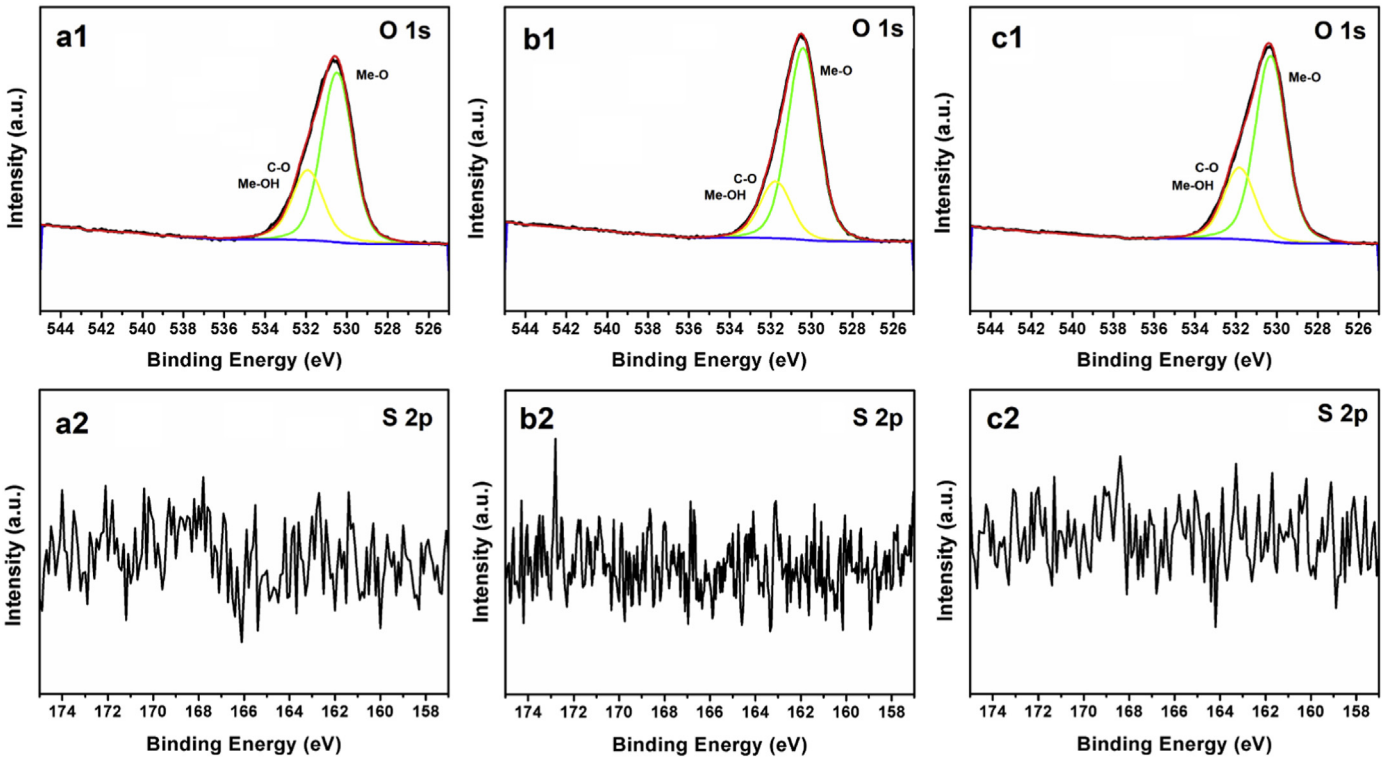

Fig. 12. High-resolution XPS of O1s and S2p for AB_5-type anodes after chronopotentiometric measurements (I = 100 mA g^{-1}) in T0 (a), T100 (b) and T1 fuel solution (c).

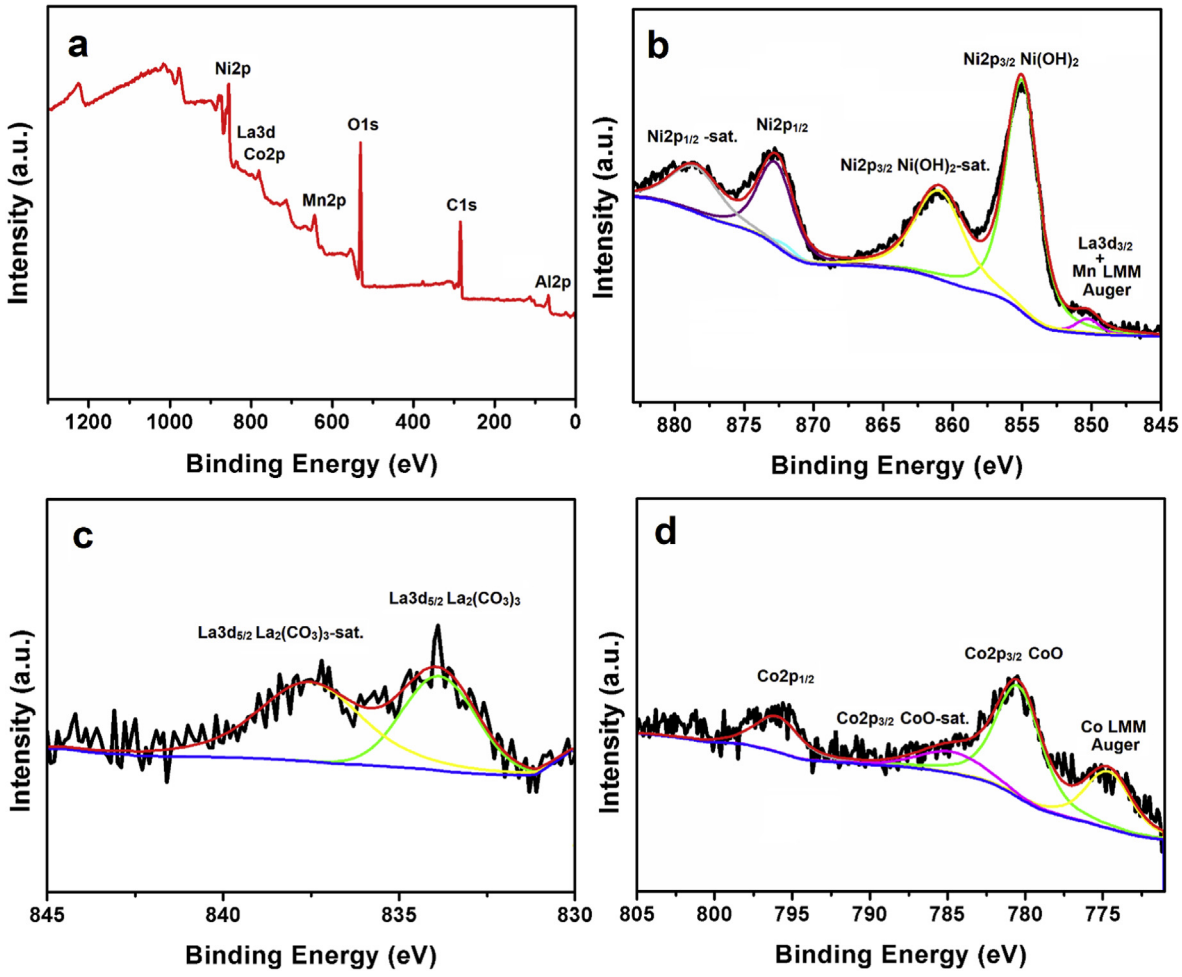

Fig. 13. Survey scanned XPS spectrum (a) high-resolution spectrum in Ni2p (b) La3d (c) and Co2p (d) for AB_5-type anodes after chronopotentiometric measurements in T0 fuel solution.

studied systems. In the lower frequency range (below 10000 Hz), the phase angle become negative. The first time constant CPE_1/R_1 (first loop or semicircle) and the second time constant CPE_2/R_2 (second loop) appeared. The third one was almost imperceptible in the lowest frequency range. In the diagram which presents the dependency of the impedance modulus and the frequency (Fig. 8b), the capacitive element of each of mentioned constants is expressed by a straight line with a slope of −1, while the resistive element corresponds to the plateau. In the case of the first and second time constants, the phase angle values were the lowest for T0 and T1 respectively, as shown in Fig. 8a.

3.2. The characterization of structure

In order to investigate the influence of immersion activation (4 h in borohydride solution with different concentrations of thiourea) on the electrode structure, XRD measurements of the analyzed electrodes were carried out. XRD patterns of anodes before (black line) and after activation in T1 fuel solution (blue line) and T0 fuel solution (red line) were presented in Fig. 9. This measurement confirmed that the AB_5-alloy-based anodes were characterized by $CaCu_5$-type hexagonal structure. It can be seen that the basic structure remains unchanged after activation. However, a slight peak shift to lower angle was observed for electrode activated in T0 solution, which is in good agreement with the results of Wang et al. [51]. This change means that the hydrogen (produced by borohydride hydrolysis process) was absorbed in the alloy during the immersion which caused the crystal expansion. No change in the

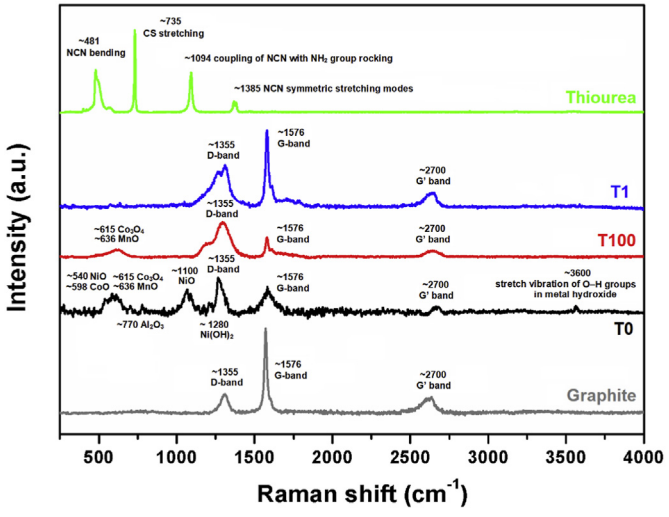

Fig. 14. Raman spectra of solid thiourea, graphite and anode materials after chronopotentiometric measurements (I = 100 mA g^{-1}) in different electrolytes.

structure of anode was observed during the electrode activation in the T1 solution, which confirms the complete inhibition of borohydride hydrolysis.

The SEM images of AB_5-alloy-based anodes before (a) and after 4 h activation in T0 (b) and T1 (c) electrolytes were presented in Fig. 10 a-c. It should be noted, that soaking of the electrode in the T0 solution results in the formation of rod-like particles on the electrode surface, which contain La, Mn or Ce elements as confirmed by EDS mapping. The presence of these particles affects the surface roughness of the alloy, which increases its active surface. Similar effects have been described by Ikoma et al. [52]. Corrosion in the T1 fuel solution was much less intense, which resulted in significantly lower surface coverage with corrosion products.

The elemental composition of the alloy has been studied by the EDS technique at different sites (1,2,3) as presented in Fig. 11 a-c. Area 1 corresponds to the graphite basis, 2 to the alloy basis and 3 to the spherical nickel particles. In area 2 (Table 4), an increase in elemental O was detected after activation in the T0 fuel solution (2b), which indicates the oxidation of electrode surface. It was found that Ni and Co decrease by a certain amount after alkaline treatment, while Al increases by an amount on the anode surface. It is well known that Mn and Al can dissolve and then deposit on the alloy surface as an oxide [51–53]. These phenomena were much less visible in the presence of thiourea (2c). This again indicates that thiourea interacts with the electrode surface, preventing corrosion. The residual amount of Pr, Ce and Nd results from the chemical composition of this alloy [54].

XPS study was carried out to obtain detailed information regarding the chemical state of the AB_5-alloy-based anodes after chronopotentiometric experiments (Fig. 12 a-c). The deconvolution of O1s spectra is in good accordance with the previously discussed results. In all cases, the anode surfaces consist of oxygen atoms with peak binding energies characteristic either for metal oxides (530.3 eV) or hydroxides and carbonates (531.8 eV) [55]. The peak for $S2p_{3/2}$, typically located at ~164 eV for metal sulfides, was not observed [56,57]. This suggests that thiourea was completely removed from the anode surface after rinsing the electrodes with distilled water.

The survey in Fig. 13a indicates the presence of the Ni, La, Co, Mn, O, C and Al peaks, which confirms the composition of the AB_5-type anode. The XPS spectrum of Ni2p (Fig. 13b) includes two characteristic peaks at 855.2 eV and 873.0 eV, which can be attributed to the spin-orbit doublet of 2p orbital of Ni^{2+} ($Ni2p_{3/2}$ and $Ni2p_{1/2}$) and two shake-up satellites at 861.2 and 879.3 eV, respectively [58]. With regard to La3d (Fig. 13c), the binding energy of the $La3d_{5/2}$ peak is present at 833.9 with the shake-up peak located at 837.6 eV, which is consistent with the reported results of La^{3+} in a La(III) oxidation state [59,60]. The Co2p spectrum (Fig. 13d) consists of the $Co2p_{3/2}$ contribution at 780.6 eV and its corresponding satellite peak at 785.2 eV as well as the $Co2p_{1/2}$ contribution at 796.2 eV, which correspond to the coexistence of Co(II) and Co(III) oxides [61,62]. Metal oxides/hydroxides are formed as a result of the consumption of oxygen in the electrolyte solution. In addition, the same chemical states are representative for each electrode tested in all fuel solutions.

Additionally, Raman spectroscopy measurements of the electrodes were performed in order to understand the process occurring at the anode surface after discharge experiments (100 mA g^{-1}) in T0, T1 and T100 fuel solutions (Fig. 14). Raman spectrum of solid thiourea is characterized by four strong bands at 481, 735, 1094 and 1385 cm^{-1}, which is in good agreement with the thiourea spectra reported in the literature [63]. These bands are assigned to NCN bending, CS stretching, strong coupling of NCN with NH_2 group rocking and NCN symmetric stretching modes, respectively. Raman spectra of the anode surface for all electrolytes exhibit two characteristic graphitic D and G-bands and one overtone G' band which appear at ~1355 cm^{-1}, ~1576 cm^{-1} and ~2700 cm^{-1}, respectively, which confirm the presence of graphite in the AB_5-alloy-based anodes [64]. Based on the literature data, the bands with a broad shoulder at approx. 500–700 cm^{-1} could be assigned to the formation of Ni, Co, Mn and Al oxides [65,66]. The band at ~1100 cm^{-1} (T0 electrolyte) can be attributed to Ni oxide, while

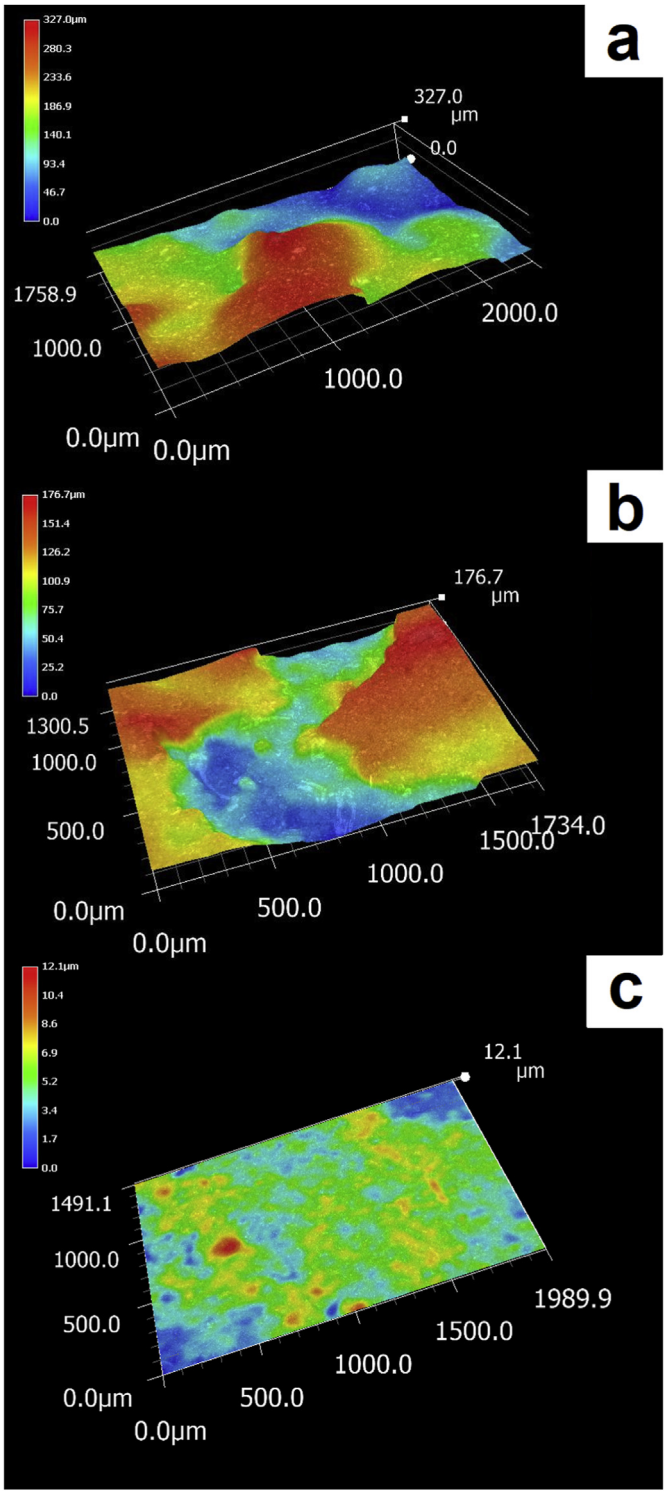

Fig. 15. 3D surface analysis of AB_5-type anodes after 4 h activation in (a) T0 (b) T100 (c) T1 fuel solutions.

bands appearing at ~1280 cm^{-1} correspond to $Ni(OH)_2$ [67]. These observations are in good agreement with the results of XPS analysis. This confirms again that thiourea reduces the formation of corrosion products. Importantly, no band originating from the metal sulphide was observed, which suggests that no poisoning of the electrode surface occurred.

Finally, 3D surface analysis also confirms that thiourea is able to inhibit the hydrogen evolution (Fig. 15 a-c). It can be observed, that nickel foam was significantly exposed after activation in the T0 solution (Fig. 15a), which corresponds to the most intense gassing in this electrolyte and, consequently, mechanical cracking of the alloy due to tension between charged and discharged alloy phases [36]. The active material was loosened and, consequently, the packing density decreased, which is an unfavorable phenomenon for DBFC application. Significantly lower loss of anode material was observed after activation in the T100 solution (Fig. 15b). The most compact and undisturbed surface was observed in case of the T1 fuel solution (Fig. 15c), which results from the completely inhibited process of borohydride hydrolysis.

4. Conclusions

Sodium borohydride hydrolysis results in a high hydrogen loss. At 100 mA g^{-1} only 27% of fuel is effectively used. It was expected that the addition of thiourea would significantly improve the coulombic efficiency by inhibiting hydrogen evolution. After addition of 0.016 mM of thiourea, the practical capacity was increased to 41%. Higher concentration of this inhibitor causes a competition between the oxidation of thiourea and borohydride. Moreover, the electrochemical data suggest that alloy hydriding occurs simultaneously with the borohydride oxidation, which significantly enhanced the catalytic performance. Pressure measurements have shown that hydrogen can be formed either by hydrolysis or by partial oxidation of borohydride ions. Raman and XPS analyses indicate that there are still no detectable elemental sulfur-rich surfaces. Taking the results of spectroscopic studies into account, it should be noted that the effect of thiourea on the AB_5 alloy-based anode remains strictly limited to adsorption/desorption phenomena without poisoning its catalytic sites.

Declaration of Competing interest

There is no conflict of interest.

CRediT authorship contribution statement

Małgorzata Graś: Conceptualization, Methodology, Validation, Investigation, Writing - original draft, Visualization. **Jarosław Wojciechowski:** Methodology, Investigation, Writing - original draft. **Katarzyna Lota:** Methodology, Resources. **Tomasz Buchwald:** Formal analysis. **Jacek Ryl:** Formal analysis, Writing - review & editing. **Grzegorz Lota:** Conceptualization, Methodology, Writing - review & editing, Supervision.

Acknowledgments

This work was financially supported by the National Science Centre (Poland) granted on the basis of decision number DEC-2017/27/N/ST8/02916.

References

[1] Y. Liang, Y. Li, H. Wang, H. Dai, Strongly coupled inorganic/nanocarbon hybrid materials for advanced electrocatalysis, J. Am. Chem. Soc. 135 (2013) 2013–2036.
[2] International Partnership for Hydrogen and Fuel Cells in the Economy IPHE Communique: Hydrogen and Fuel Cells: A Clean, Real and Global Opportunity, 2017. http://www.iphe.net/docs/Communique%202015-12-01%20Final.pdf. accessed 13 December 2017.
[3] T. Maiyalagan, V.S. Saji, Electrocatalysts for Low Temperature Fuel Cells, Wiley-VCH, Weinheim, 2017.
[4] E.H. Yu, X. Wang, U. Krewer, L. Li, K. Scott, Direct oxidation alkaline fuel cells: from materials to systems, Energy Environ. Sci. 5 (2012) 5668–5680.
[5] D. Kong, X. Ni, C. Dong, L. Zhang, C. Man, J. Yao, K. Xiao, X. Li, Heat treatment effect on the microstructure and corrosion behavior of 316L stainless steel fabricated by selective laser melting for proton exchange membrane fuel cells, Electrochim. Acta 276 (2018) 293–303.
[6] D. Kong, C. Dong, X. Ni, L. Zhang, H. Luo, R. Li, L. Wang, C. Man, X. Li, Superior resistance to hydrogen damage for selective laser melted 316l stainless steel in a proton exchange membrane fuel cell environment, Corrosion Sci. In press, https://doi.org/10.1016/j.corsci.2019.108425.
[7] D.M.F. Santos, C.A.C. Sequeira, Sodium borohydride as a fuel for the future, Renew. Sustain. Energy Rev. 15 (2011) 3980–4001.
[8] C. Ponce de León, F.C. Walsh, D. Pletcher, D.J. Browning, J.B. Lakeman, Direct borohydride fuel cells, J. Power Sources 155 (2006) 172–181.
[9] C.J. Lee, T. Kim, Hydrogen supply system employing direct decomposition of solid-state $NaBH_4$, Int. J. Hydrogen Energy 40 (2015) 2274–2282.
[10] R. Jamard, A. Latour, J. Salomon, P. Capron, A. Martinent-Beaumont, Study of fuel efficiency in a direct borohydride fuel cell, J. Power Sources 176 (2008) 287–292.
[11] B.H. Liu, Z.P. Li, S. Suda, Anodic oxidation of alkali borohydrides catalyzed by nickel, J. Electrochem. Soc. 150 (2003) A398–A402.
[12] K. Wang, K. Jiang, J. Lu, L. Zhuang, C. Cha, X. Hu, G.Z. Chen, Eight-electron oxidation of borohydride at potentials negative to reversible hydrogen electrode, J. Power Sources 185 (2008) 892–894.
[13] X. Yang, Y. Liu, S. Li, X. Wei, L. Wang, Y. Chen, A direct borohydride fuel cell with a polymer fiber membrane and non-noble metal catalysts, Sci. Rep. 2 (2012) 567.
[14] G. Behmenyar, A.N. Akin, Investigation of carbon supported Pd-Cu nanoparticles as anode catalysts for direct borohydride fuel cell, J. Power Sources 249 (2014) 239–246.
[15] G. Lota, A. Sierczynska, I. Acznik, K. Lota, AB_5-type Hydrogen storage alloy modified with carbon used as anodic materials in borohydride fuel cells, Int. J. Electrochem. Sci. 9 (2014) 659–669.
[16] M. Martins, B. Šljukć, C.A.C. Sequeira, Ö. Metin, M. Erdem, T. Sener, D.M.F. Santos, Biobased carbon-supported palladium electrocatalysts for borohydride fuel cells, Int. J. Hydrogen Energy 41 (2016) 10914–10922.
[17] C. Grimmer, R. Zacharias, M. Grandi, B. Pichler, I. Kaltenboeck, F. Gebetsroither, J. Wagner, B. Cermenek, S. Weinberger, A. Schenk, V. Hacker, A membrane-free and practical mixed electrolyte direct borohydride fuel cell, J. Electrochem. Soc. 163 (2016) F278–F283.
[18] K. Wang, K. Jiang, J. Lu, L. Zhuang, C. Cha, X. Hu, G.Z. Chen, Eight-electron oxidation of borohydride at potentials negative to reversible hydrogen electrode, J. Power Sources 185 (2008) 892–894.
[19] G. Wang, X. Wang, R. Miao, D. Cao, K. Sun, Effects of alkaline treatment of hydrogen storage alloy on electrocatalytic activity for $NaBH_4$ oxidation, Int. J. Hydrogen Energy 35 (2010) 1227–1231.
[20] E. Gyenge, Electrooxidation of borohydride on platinum and gold electrodes: implications for direct borohydride fuel cells, Electrochim. Acta 49 (2004) 965–978.
[21] U.B. Demirci, Comments on the paper "Electrooxidation of borohydride on platinum and gold electrodes: implications for direct borohydride fuel cell" by E. Gyenge, Electrochim. Acta 49 (2004) 965: thiourea, a poison for the anode metallic electrocatalyst of the direct borohydride fuel cell? Electrochim. Acta 52 (2007) 5119–5121.
[22] R. Holze, S. Schomaker, New results on the electrosorption of urea and thiourea on gold electrodes, Electrochim. Acta 35 (1990) 613–620.
[23] G. Garcia, J.L. Rodriguez, G.I. Lacconi, E. Pastor, Spectroscopic investigation of the adsorption and oxidation of thiourea on polycrystalline Au and Au (111) in acidic media, Langmuir 20 (2004) 8773–8780.
[24] A.E. Bolzan, R.C.V. Piatti, R.C. Salvarezza, A.J. Arvia, Electrochemical study of thiourea and substituted thiourea adsorbates on polycrystalline platinum electrodes in aqueous sulfuric acid, J. Appl. Electrochem. 32 (2002) 611–620.
[25] J.Z. Zheng, B. Ren, D.Y. Wu, Z.Q. Tian, Thiourea adsorption on a Pt surface as detected by electrochemical methods and surface-enhanced Raman spectroscopy, J. Electroanal. Chem. 574 (2005) 285–289.
[26] G. Garcia, J.L. Rodriguez, G.I. Lacconi, E. Pastor, Adsorption and oxidation pathways of thiourea at polycrystalline platinum electrodes, J. Electroanal. Chem. 588 (2006) 169–178.
[27] A. Lukomska, S. Smolinski, J. Sobkowski, Adsorption of thiourea on monocrystalline copper electrodes, Electrochim. Acta 46 (2001) 3111–3117.
[28] M. Fleischmann, I.R. Hill, G. Sundholm, A Raman spectroscopic study of thiourea adsorbed on silver and copper electrodes, J. Electroanal. Chem. Interfacial Electrochem. 157 (1983) 359–368.
[29] Z.Q. Tian, Y.Z. Lian, M. Fleischmann, In-situ Raman spectroscopic studies on coadsorption of thiourea with anions at silver electrodes, Electrochim. Acta 35 (1990) 879–883.
[30] J. Bukowska, K. Jackowska, Influence of thiourea on hydrogen evolution at a silver electrode as studied by electrochemical and SERS methods, J. Electroanal. Chem. 367 (1994) 41–48.

[31] C. Celik, F.G. Boyaci San, H.I. Sarac, Improving the direct borohydride fuel cell performance with thiourea as the additive in the sodium borohydride solution, Int. J. Hydrogen Energy 35 (2010) 8678–8682.
[32] V.W.S. Lam, D.C.W. Kannangara, A. Alfantazi, E.L. Gyenge, Electrochemical quartz crystal microbalance study of borohydride electro-oxidation on Pt: the effect of borohydride concentration and thiourea adsorption, J. Phys. Chem. C 115 (2011) 2727–2737.
[33] E.L. Gyenge, Reply to "Comments on the paper ['Electrooxidation of borohydride on platinum and gold electrodes: implications for direct borohydride fuel cells' by E. Gyenge, Electrochim. Acta 49 (2004) 965]: thiourea, a poison for the anode metallic electrocatalyst of the direct borohydride fuel cell?" by U.B. Demirci, Electrochim. Acta 52 (2007) 5122–5123.
[34] M.H. Atwan, D.O. Northwood, E.L. Gyenge, Evaluation of colloidal Os and Os-alloys (Os-Sn, Os-Mo and Os-V) for electrocatalysis of methanol and borohydride oxidation, Int. J. Hydrogen Energy 30 (2005) 1323–1331.
[35] M. Graś, A. Sierczyńska, K. Lota, I. Acznik, G. Lota, The modification of anode material for direct borohydride fuel cell, Ionics 22 (2016) 2539–2544.
[36] M. Karwowska, K.J. Fijalkowski, A. Czerwiński, Corrosion of hydrogen storage metal alloy LaMm-$Ni_{4.1}Al_{0.3}Mn_{0.4}Co_{0.45}$ in the aqueous solutions of alkali metal hydroxides, Materials 11 (2018) 2423.
[37] K. Szubert, J. Wojciechowski, J. Karasiewicz, H. Maciejewski, G. Lota, Corrosion-protective coatings based on fluorocarbosilane, Prog. Org. Coating 123 (2018) 374–383.
[38] J. Wojciechowski, Ł. Kolanowski, A. Bund, G. Lota, The influence of current collector corrosion on the performance of electrochemical capacitors, J. Power Sources 368 (2017) 18–29.
[39] J. Wojciechowski, K. Szubert, R. Peipmann, M. Fritz, U. Schmidt, A. Bund, G. Lota, Anti-corrosive properties of silane coatings deposited on anodised aluminium, Electrochim. Acta 220 (2016) 1–10.
[40] K. Szubert, J. Wojciechowski, J. Karasiewicz, H. Maciejewski, G. Lota, Corrosion protection of stainless steel by triethoxyoctylsilane and tetraethoxysilane, Int. J. Electrochem 11 (2016) 8256–8269.
[41] R.T. Loto, C.A. Loto, A.P.I. Popoola, Corrosion inhibition of thiourea and thiadiazole derivatives: a review, J. Mater. Environ. Sci. 3 (2012) 885–894.
[42] W. J Paschoalino, E.A. Ticianelli, An investigation of the borohydride oxidation reaction on La-Ni-based hydrogen storage alloys, Int. J. Hydrogen Energy 38 (2013) 7344–7352.
[43] L. Wang, G. Wu, Z. Yang, Y. Gao, X. Mao, C. Ma, Electrochemical characteristics of $LaNi_{4.5}$ $Al_{0.5}$ alloy used as anodic catalyst in a direct borohydride fuel cell, J. Mater. Sci. Technol. 27 (2011) 46–50.
[44] I. Merino-Jiménez, C. Ponce de León, A.A. Shah, F.C. Walsh, Developments in direct borohydride fuel cells and remaining challenges, J. Power Sources 219 (2012) 339–357.
[45] J.I. Martins, M.C. Nunes, R. Koch, L. Martins, M. Bazzaoui, Electrochemical oxidation of borohydride on platinum electrodes: the influence of thiourea in direct fuel cells, Electrochim. Acta 52 (2007) 6443–6449.
[46] M. Graś, Ł. Kolanowski, J. Wojciechowski, G. Lota, Electrochemical supercapacitor with thiourea-based aqueous electrolyte, Electrochem. Commun. 97 (2018) 32–36.
[47] P.J. Vandeberg, D.C. Johnson, A study of the voltammetric response of thiourea and ethylene thiourea at gold electrodes in alkaline media, J. Electroanal. Chem 362 (1993) 129–139.
[48] R.N. Bulakhe, S. Sahoo, T.T. Nguyen, D.L. Chandrakant, D. Lokhande, R. Changhyun, Y.R. Lee, J.-J. Shim, Chemical synthesis of 3D copper sulfide with different morphologies for high performance supercapacitors application, RSC Adv. 6 (2016) 14844–14851.
[49] A. Lasia, Electrochemical Impedance Spectroscopy and its Applications, Springer, New York, 2014.
[50] P. Slepski, K. Darowicki, M. Kopczyk, A. Sierczynska, K. Andrearczyk, Electrochemical impedance studies of AB_5-type hydrogen storage alloy, J. Power Sources 195 (2010) 2457–2462.
[51] G. Wang, X. Wang, R. Miao, D. Cao, K. Sun, Effects of alkaline treatment of hydrogen storage alloy on electrocatalytic activity for $NaBH_4$ oxidation, Int. J. Hydrogen Energy 35 (2010) 1227–1231.
[52] M. Ikoma, K. Komori, S. Kaida, C. Iwakura, Effect of alkali-treatment of hydrogen storage alloy on the degradation of Ni/MH batteries, J. Alloys Compd. 284 (1999) 92–98.
[53] J. Wysocka, S. Krakowiak, J. Ryl, K. Darowicki, Investigation of the electrochemical behaviour of AA1050 aluminium alloy in aqueous alkaline solutions using Dynamic Electrochemical Impedance Spectroscopy, J. Electroanal. Chem. 778 (2016) 126–136.
[54] K. Lota, A. Sierczyńska, G. Lota, Synthesis and electrochemical properties of carbon nanotubes obtained by pyrolysis of acetylene using AB_5 alloy, J. Solid State Electrochem. 14 (2010) 2209–2212.
[55] J. Ryl, M. Brodowski, M. Kowalski, W. Lipinska, P. Niedzialkowski, J. Wysocka, Corrosion inhibition mechanism and efficiency differentiation of dihydroxybenzene isomers towards aluminum alloy 5754 in alkaline media, Materials 12 (2019) 3067.
[56] J. Chen, H. Zhang, P. Liu, Y. Li, G. Li, T. An, H. Zhao, Thiourea sole doping reagent approach for controllable N, S co-doping of pre-synthesized large-sized carbon nanospheres as electrocatalyst for oxygen reduction reaction, Carbon 92 (2015) 339–347.
[57] D. Chen, R. Yang, L. Chen, Y. Zou, B. Ren, L. Li, S. Li, Y. Yan, Y. Xu, One-pot fabrication of nitrogen and sulfur dual-doped graphene/sulfur cathode via microwave assisted method for long cycle-life lithium-sulfur batteries, J. Alloys Compd. 746 (2018) 116–124.
[58] H. Liu, Q. He, H. Jiang, Y. Lin, Y. Zhang, M. Habib, S. Chen, L. Song, Electronic structure reconfiguration toward pyrite NiS_2 via engineered heteroatom defect boosting overall water splitting, ACS Nano 11 (2017) 11574–11583.
[59] J.-G. Kang, Y.-I. Kim, D.W. Cho, Y. Sohn, Synthesis and physicochemical properties of $La(OH)_3$ and La_2O_3 nanostructures, Mater. Sci. Semicond. Process. 40 (2015) 737–743.
[60] S. Chen, B. Pan, L. Zeng, S. Luo, X. Wang, W. Su, $La_2Sn_2O_7$ enhanced photocatalytic CO_2 reduction with H_2O by deposition of Au co-catalyst, RSC Adv. 7 (2017) 14186–14191.
[61] M. Tong, L. Wang, P. Yu, X. Liu, H. Fu, 3D Network nanostructured NiCoP nanosheets supported on N-doped carbon coated Ni foam as a highly active bifunctional electrocatalyst for hydrogen and oxygen evolution reactions, Front. Chem. Sci. Eng. 12 (2018) 417–424.
[62] C. Fettkenhauer, X. Wang, K. Kailasam, M. Antonietti, D. Dontsova, Synthesis of efficient photocatalysts for water oxidation and dye degradation reactions using $CoCl_2$ eutectics, J. Mater. Chem. A. 3 (2015) 21227–21232.
[63] P. Cao, J. Yao, B. Ren, R. Gu, Z. Tian, Surface-enhanced Raman scattering spectra of thiourea adsorbed at an iron electrode in $NaClO_4$ solution, J. Phys. Chem. B 106 (2002) 10150–10156.
[64] A. Singh, A.J. Roberts, R.C.T. Slade, A. Chandra, High electrochemical performance in asymmetric supercapacitors using MWCNT/nickel sulfide composite and graphene nanoplatelets as electrodes, J. Mater. Chem. A2 (2014) 16723–16730.
[65] J. Nan, Y. Yang, Z. Lin, Raman spectroscopic study on the surface oxide layer of AB_5-type metal hydride electrodes, Electrochim. Acta 46 (2001) 1767–1772.
[66] P.V. Thomas, V. Ramakrishnan, V.K. Vaidyan, Oxidation studies of aluminium thin films by Raman spectroscopy, Thin Solid Films 170 (1989) 35–40.
[67] M.E. Plonska-Brzezinska, D.M. Brus, A. Molina-Ontoria, L. Echegoyen, Synthesis of carbon nano-onion and nickel hydroxide/oxide composites as supercapacitor electrodes, RSC Adv. 3 (2013) 25891–25901.